



## Research articles

# Magneto-optical spectroscopy of diluted magnetic semiconductors GaMnAs prepared by ion implantation and further impulse laser annealing



E.A. Gan'shina<sup>a,\*</sup>, L.L. Golik<sup>b</sup>, Z.E. Kun'kova<sup>b</sup>, G.S. Zykov<sup>a</sup>, I.V. Bykov<sup>c</sup>, A.I. Rukovishnikov<sup>b</sup>, Ye Yuan<sup>d</sup>, R. Böttger<sup>d</sup>, S. Zhou<sup>d</sup>

<sup>a</sup> Department of Physics, Lomonosov Moscow State University, Moscow, Russia

<sup>b</sup> Kotelnikov Institute of Radioengineering and Electronics (Fryazino Branch), RAS, Fryazino, Russia

<sup>c</sup> Institute for Theoretical and Applied Electrodynamics, RAS, Moscow, Russia

<sup>d</sup> Helmholtz-Zentrum Dresden Rossendorf, Institute of ion-beam science and Materials Research, Dresden, Germany

## ARTICLE INFO

## Article history:

Received 10 July 2017

Received in revised form 17 October 2017

Accepted 14 November 2017

Available online 15 November 2017

## Keywords:

GaMnAs

Magneto-optics

Ellipsometry

Ion implantation

Laser annealing

## ABSTRACT

Ga<sub>1-x</sub>Mn<sub>x</sub>As layers prepared by ion implantation and subsequent pulsed laser annealing with the planned Mn concentrations of  $x = 0.01$ – $0.08$  have been studied using the magneto-optical transversal Kerr effect (TKE) and spectral ellipsometry. The spectral dependences of the diagonal and nondiagonal components of the permittivity tensor (PT), as well as the spectrum of magnetic circular dichroism (MCD) have been calculated for the layers. The obtained spectra of the diagonal PT components show that the layers under study maintain the zinc-blende crystal structure of the parent GaAs semiconductor. All studied samples reveal a strong TKE response at low temperatures with a dependence of an effective Curie temperature (at which TKE appears) on the Mn concentration. A number of extrema in the low-temperature TKE and MCD spectra are close to the energies of transitions in the  $\Gamma$  and L critical points of the parent semiconductor band structure that confirms the intrinsic ferromagnetism of the Ga<sub>1-x</sub>Mn<sub>x</sub>As layers. The MCD spectra shape and its change with Mn concentration increasing are discussed on a base of the valence-band model of ferromagnetism in DMS.

© 2017 Published by Elsevier B.V.

## 1. Introduction

The (Ga,Mn)As diluted magnetic semiconductor (DMS) is the model object both for ascertainment of the nature of ferromagnetic coupling in the (III,Mn)V DMS and for control of their magnetic properties. However, despite the intensive research the debates regarding the electronic states near the top of the valence band and at the Fermi energy as well as the exchange mechanisms leading to ferromagnetic ordering still continue [1–3]. Some authors assume that in heavily doped ferromagnetic (Ga,Mn)As the Fermi level lies in the narrow impurity band separated by an energy gap from the valence band, and the metallic conductivity of such samples is due to the hole motion along the impurity band (the IB-hole model) [4–8]. At the same time, according to [9–12], there is no the impurity band detached from the valence band in ferromagnetic metallic (Ga,Mn)As samples, and the Fermi level is located in the valence band (the VB-hole model).

In parallel with probing the spectrum of electronic states magneto-optical (MO) spectroscopy allows one to detect and identify various magnetic phases, which can be present in (Ga,Mn)As samples. Magnetic circular dichroism (MCD) is usually considerably enhanced around the critical points of semiconductor band structure [13], therefore MCD spectroscopy is especially widely exploited. However, the experimental MCD data available in the literature are interpreted by authors from different research groups as evidences supporting both points of view.

Low-temperature molecular beam epitaxy (LT-MBE) is the most common way to obtain (III,Mn)V systems [14,15] and the majority of studies has been performed on LT-MBE (Ga,Mn)As samples. In the course of the low-temperature growth the point defects (interstitial Mn and antisite As) arise, which, being donors, compensate largely the majority carriers (holes) and reduce the ferromagnetic ordering temperature,  $T_C$ , of (Ga,Mn)As. The discrepancies between the experimental results of different authors, apparently, are related to the problem of fabrication of the samples with well-controlled defects.

\* Corresponding author.

E-mail address: [eagan@mail.ru](mailto:eagan@mail.ru) (E.A. Gan'shina).

The other growth techniques such as metal organic vapour phase epitaxy (MOVPE) [16], ion implantation and subsequent pulsed laser annealing [17,18] as well as pulsed laser deposition [19] are also used to prepare (Ga,Mn)As layers. In the case of these methods, other defect types may arise during the growth process that can have a significant impact on the character of impurity states, concentration of itinerant holes and the Fermi level location. Therefore, studies of (Ga,Mn)As grown by the alternative methods can provide additional information on the details of the (Ga,Mn)As electronic structure, particularly about the Fermi level position.

In our previous studies [20–22] the MO technique (the transversal Kerr effect, TKE) was used together with spectral ellipsometry to characterize the IIIMnV layers (III = Ga, In; V = As) grown by laser deposition. It has been ascertained that these layers contain ferromagnetic MnAs inclusions, which appreciably determine the layers properties, in particular their strong MO response at room temperature. In the TKE spectra of such layers both the structures associated with the optical transitions in “bulk” MnAs inclusions and the resonant TKE band ( $E = 0.5–2.0$  eV) conditioned by excitation of the surface plasmons can be present. The knowledge about these spectra features allows one to detect the presence of the undesirable MnAs phase in Ga(In)MnAs layers.

In this paper, we present results of the investigations of magneto-optical and optical properties of GaMnAs layers fabricated by ion implantation and subsequent pulsed laser annealing. The results show that the MnAs phase is absent in our samples. The samples demonstrate ferromagnetic behaviour at low temperatures. We have calculated spectra of the real and imaginary parts,  $\varepsilon'_1(E)$  and  $\varepsilon''_2(E)$ , of the nondiagonal components of the permittivity tensor as well as spectra of the magnetic circular dichroism for samples under study and compared them with the published MCD spectra of (Ga,Mn)As grown by LT-MBE [5,6,10,23–26]. Features in the MCD and TKE spectra of our samples and their change with increasing Mn concentration are explained on a base of the valence-band model of ferromagnetism in DMS, taking into account the electronic phase separation and quantum size effect.

## 2. Material and methods

### 2.1. Ion implantation and further impulse laser annealing

The  $\text{Ga}_{1-x}\text{Mn}_x\text{As}$  layers on GaAs(001) substrates were prepared by ion implantation at room temperature at the Ion Beam Center at the Helmholtz-Zentrum Dresden-Rossendorf. Mn ions were implanted into intrinsic GaAs(001) wafers at the energy of 100 keV at an incidence angle of  $7^\circ$  to avoid ion channeling. According to SRIM simulations, the Mn concentration was planned to be from 0.01 to 0.08 considering fluence of  $1 \times 10^{15}–2 \times 10^{16}$   $\text{cm}^{-2}$ . A coherent XeCl excimer laser with 308 nm wavelength and 28 ns duration was used to anneal the implanted GaAs layer. The profile of the laser beam was homogenized to  $5 \times 5$   $\text{mm}^2$ . The annealing energy was optimized to be 0.3 J/ $\text{cm}^2$ . However, the laser annealing made the amount of implanted Mn atoms (inside the GaAs layer) diverged from the planned value, because part of the implanted Mn atoms diffused to the surface during the recrystallization procedure. Later on, the sample surface was etched in concentrated HCl to remove the inert surface layer. Nevertheless, substantial part of the Mn atoms still remained inside the GaAs matrix. The Mn concentration was measured by secondary ions mass spectrometry (SIMS) and it was determined by the obtained peak value. Fabrication conditions,  $x$  values planned and determined by SIMS, samples spontaneous magnetization,  $M_s$ , and thickness as well as Curie temperature magnitudes,  $T_c$ , got from magnetometry, magneto-optical and electrical measurements are presented in Table 1. Magnetometry was performed

using a SQUID-VSM magnetometer from Quantum Design. More details about the samples fabrication are shown in Ref. [17,18]. Data of SIMS and cross-sectional high-resolution TEM as well as of magnetometry and electrical measurements for the given samples are presented in our work [27].

### 2.2. Magneto-optical and optical spectroscopy

Magneto-optical transversal Kerr effect, TKE, consists in an intensity variation of the p-polarized light reflected by a sample under magnetization. The value  $\delta = [I(H) - I(-H)]/2I(0)$ , where  $I(H)$  and  $I(0)$  are the reflected light intensities in the presence and absence of a magnetic field, respectively, was directly measured in the experiment. The alternating magnetic field up to 240 kA/m was aligned parallel to the sample surface and perpendicular to the light incidence plane. The sensitivity of the apparatus was  $\approx 10^{-5}$ . The TKE spectra,  $\delta(E)$ , were recorded in the energy range of  $E = 0.5–4.0$  eV. The temperature range for the studies was  $T = 15–300$  K. The TKE value depends linearly on magnetization and we have measured temperature dependences,  $\delta(T)$ , as well as TKE dependences on magnetic field,  $\delta(H)$ , at some fixed energies to characterize magnetic state of the layers.

To record the ellipsometry parameters spectra,  $\tan\psi(E)$  and  $\cos\Delta(E)$ , we employed the ellipsometer SE 850 DUV SENTECH Instruments GmbH (the energy range of  $E = 0.55–6.5$  eV, samples #1 – #3, #6,) and ellipsometer with binary modulation of light polarization state [28] ( $E = 1.24–4.5$  eV, samples #4 and #5). The spectra were recorded at room temperature.

## 3. Results

### 3.1. Spectral ellipsometry

We used the ellipsometry spectra,  $\tan\psi(E)$  and  $\cos\Delta(E)$ , to derive the spectral dependences of the real and imaginary parts,  $\langle\varepsilon_1\rangle$  and  $\langle\varepsilon_2\rangle$ , respectively, of the diagonal components of the pseudo-dielectric function<sup>1</sup>, for the samples investigated. The obtained  $\langle\varepsilon_1\rangle(E)$  and  $\langle\varepsilon_2\rangle(E)$  spectra are shown in Fig. 1. Dashed lines show the energies of the transitions at the  $\Gamma$ - and L-critical points of GaAs at room temperature [30]. As is clear from Fig. 1, peaks corresponding to the optical transitions near the L critical point of the Brillouin zone of GaAs are present in the  $\langle\varepsilon_2\rangle(E)$  spectrum of all  $\text{Ga}_{1-x}\text{Mn}_x\text{As}$  samples. Therefore, we can conclude that the crystal structure of the GaAs parent semiconductor is conserved in the layers under study. An increase in matrix imperfection when the Mn dopant is introduced is a possible reason for decreasing the maxima and smearing the doublet ( $E \approx 2.9–3.2$  eV), as well as for the increase in the  $\langle\varepsilon_2\rangle$  values in the region  $E \approx 1.2–2.9$  eV. The transformation of the  $\langle\varepsilon_1\rangle(E)$  and  $\langle\varepsilon_2\rangle(E)$  dependences in the energy region  $E < 3$  eV is also associated with the light interference in the  $\text{Ga}_{1-x}\text{Mn}_x\text{As}$  layers. The interference contribution appears and rises below the  $E_1$  transition energy, where the optical absorption in the semiconducting matrix abruptly decreases and the depth of the light penetration into the sample increases. The interference fringes are especially well marked in the spectra of sample #6. In Fig. 1 arrows denote these fringes.

A possible reason for the interference in sample #6 can be its relatively high transmission in the range  $E < 3$  eV. Note that the structures associated with the transitions  $E_1$  and  $E_1 + \Delta_1$  in the spectra of this sample are smeared weaker than those in the other samples spectra. This is apparently due to smaller imperfection of

<sup>1</sup> The pseudo-dielectric function is obtained directly from the measured  $\tan\psi$  and  $\cos\Delta$  values with the use of the optical model assuming a flat substrate with infinite thickness [29].

**Table 1**

Fabrication conditions, Mn concentration planned,  $x$ , and determined by SIMS,  $X_{\text{peak}}$ , samples spontaneous magnetization,  $M_s$ , and thickness as well as Curie temperature magnitudes from magnetic, magneto-optical and electrical measurements.

Sample number, $N$	#1	#2	#3	#4	#5	#6
Mn concentration, $x$ (%), SRIM simulation	$\approx 1$	$\approx 1.5$	$\approx 2$	$\approx 4$	$\approx 6$	$\approx 8$
$X_{\text{peak}}$ from SIMS (%)	0.66	0.87	1.2	1.8	–	–
Implanting fluence ( $\text{cm}^{-2}$ )	$1 \times 10^{15}$	$1.5 \times 10^{15}$	$2 \times 10^{15}$	$8 \times 10^{15}$	$1 \times 10^{16}$	$2 \times 10^{16}$
XeCl excimer laser, $\lambda = 308$ nm, $\tau = 28$ ns, Annealing energy ( $\text{J}/\text{cm}^2$ )	0.3	0.3	0.3	0.3	0.3	0.3
$T_C$ from $M(T)$ measurements (K) [	7.5	17	31	60	60	95
$T_C$ from TKE( $T$ )** measurements (K)	–	40	55	75	80	95
$T_C$ from $R(T)$ measurements (K) ( $T_{R\text{max}}$ )	–	–	30	50	63	95
$M_s$ ( $\text{emu}/\text{cm}^3$ )	2.8	5.0	7.75	14.0	26.7	33.3
Layer thickness (nm)	60	60	60	60	60	$\sim 100^*$

\*The estimation obtained using an interference pattern in optical spectra of sample #6 (see below).

\*\* $T_C$ – an effective Curie temperature determined by the start of abrupt TKE rise when  $T$  decreases.

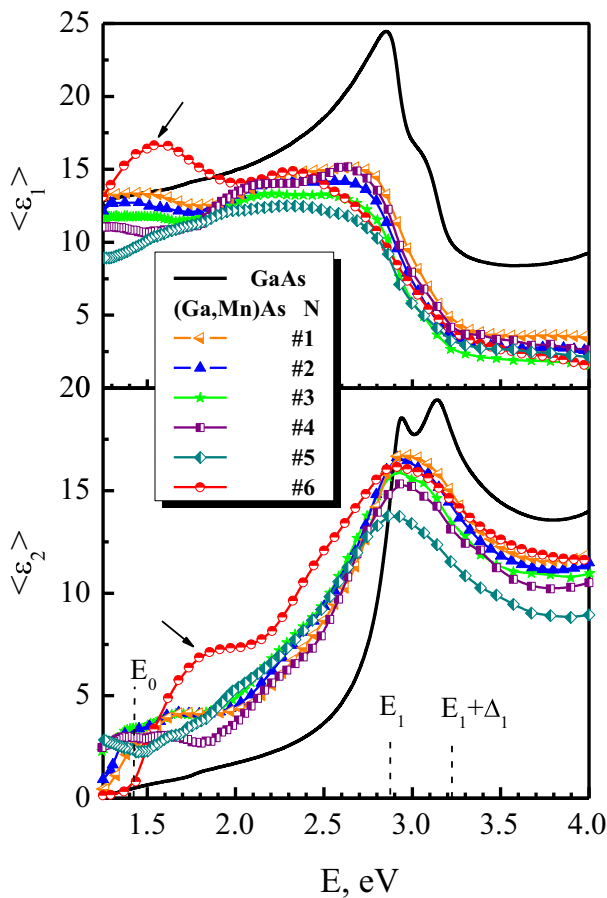


**Fig. 1.** Spectral dependences of the real and imaginary parts of the pseudo-dielectric function,  $\langle \epsilon_1 \rangle(E)$  and  $\langle \epsilon_2 \rangle(E)$ , respectively, for  $\text{Ga}_{1-x}\text{Mn}_x\text{As}$  samples #1 – #6 at  $T = 295$  K.  $\epsilon_1(E)$  and  $\epsilon_2(E)$  spectra computed for an GaAs layer using the tabulated data [26] are shown for comparison. Dashed lines show the energies of the transitions at the  $\Gamma$ - and  $L$ - critical points of GaAs at room temperature [30].

the crystal lattice in sample #6. In addition, for sample #6 we were able to simulate the ellipsometry spectra using a two-layer model that testifies to its relatively high homogeneity across the thickness and less light scattering in it.

### 3.2. Transversal Kerr effect

TKE spectra,  $\delta(E)$ , for samples #1 – #6 measured at  $T = 17$  K and light incidence angle of  $\varphi = 68^\circ$  are shown in Fig. 2. One can see

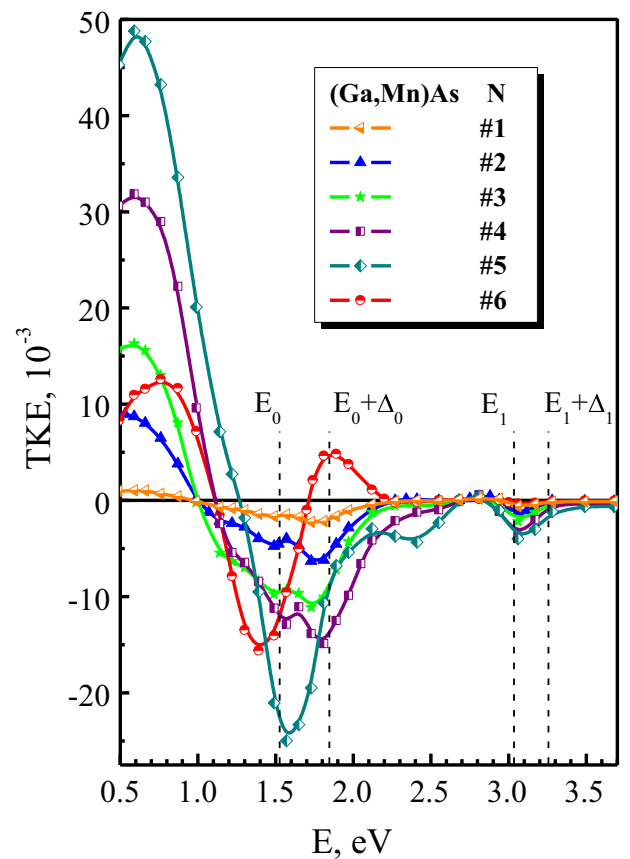


**Fig. 2.** TKE spectra of  $\text{Ga}_{1-x}\text{Mn}_x\text{As}$  samples #1 – #6 at  $T = 17$  K and  $\varphi = 68^\circ$ . Dashed lines show the energies of the  $E_0$ ,  $E_0 + \Delta_0$  and  $E_1$ ,  $E_1 + \Delta_1$  transitions in GaAs at  $T = 22$  K [31].

that the TKE spectra of samples #1 – #4 are similar. There is a negative polarity band with two local minima near the energies of  $E_0$  and  $E_0 + \Delta_0$  transitions ( $\approx 1.5$  and  $1.8$  eV) in the range  $E < 2.5$  eV. In the impurity region,  $E < 1.2$  eV, a positive TKE band is observed. As the Mn concentration increases, these features increase monotonically, and a weak blue shift of the negative local extrema takes place. In the spectrum of sample #5, along with a significant increase in the TKE signal, a change in the negative band shape is observed. Instead of two minima, there is one negative peak near 1.6 eV in the spectrum of sample #5. In the spectra of all samples, there is a negative band in the region of  $E_1$ ,  $E_1 + \Delta_1$  transitions in GaAs. This band rises with increase of the Mn concentration,

without changing the shape, in the spectra of samples #1 – #5. Sample #6 with the highest Mn concentration represents an exception. The TKE response of sample #6 in the region of the  $E_1, E_1 + \Delta_1$  transitions is weaker than one of the other samples. In addition, its TKE spectrum differs appreciably from the spectra of samples #1 – #5 in the range  $E < 2.5$  eV.

Note that the TKE spectra of the Mn-doped GaAs samples prepared by ion implantation and laser annealing significantly differ in shape from those of the GaMnAs samples with MnAs inclusions, which have been prepared by laser ablation [20–22]. In the spectra shown in Fig. 2 the TKE extrema are located close to the energies of the transitions at the critical points of the “parent” semiconductor band structure that confirms the intrinsic ferromagnetism of the layers under study.

The temperature and field dependences of the TKE response have shown that all samples with  $x > 1\%$  demonstrate ferromagnetic behaviour at low temperatures. Dependences of reduced saturation magnetization,  $M/M_s$ , on magnetic field derived from the  $\delta(H)$  those as well as temperature TKE dependences,  $\delta(T)$ , at fixed energies are displayed for some samples in Fig. 3(a, b), respectively.

The effective Curie temperature determined from the  $\delta(T)$  curves rises with increasing the Mn concentration. For samples #1–#5 it is slightly higher than the  $T_C$  value obtained from the remanent magnetization measurements in zero magnetic field [27], Table 1. This distinction can be caused by the magnetic ordering of nano-sized ferromagnetic clusters (arising in samples at temperatures a little exceeding  $T_C$ ) by a magnetic field applied when TKE is measured. As a consequence, the detected magneto-optical signal will show a ferromagnetic-like behaviour above  $T_C$  obtained from measurements in zero field. In addition, for the samples with inhomogeneous distribution of free carriers (electron phase separation [27]) the TKE measurements may detect the contribution from a small number of local regions with an increased carrier concentration and  $T_C$ , which are localized in the near-surface layer. Note that for metallic sample #6 (which differs by a higher optical homogeneity) the difference in the  $T_C$  values is absent.

We did not observe any MO response at room temperature that together with the TKE spectra character points to the absence of MnAs clusters in our samples.

#### 4. Discussion

We performed simulation of the TKE spectra by varying the shape and spectral position of contours of the real and imaginary

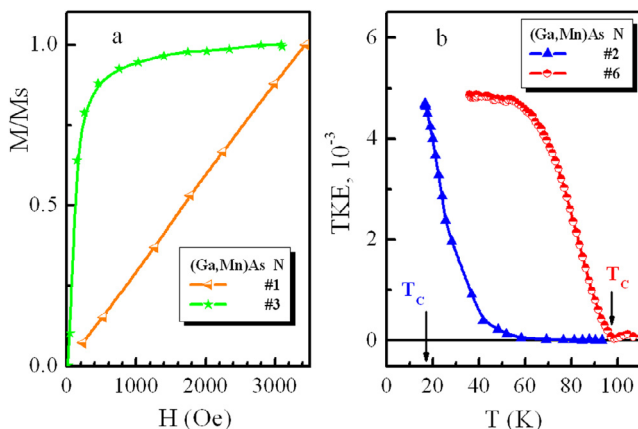


**Fig. 3.** (a) Dependences of the reduced magnetization,  $M/M_s$ , on magnetic field for samples #1 and #3,  $T = 16$  K. (b) Temperature TKE dependences for samples #2 and #6 measured at  $E = 1.9$  eV. Arrows indicate the Curie temperature values obtained from the magnetic measurements.

parts of the nondiagonal components of the permittivity tensor,  $\epsilon'_1(E)$  and  $\epsilon'_2(E)$ , and using the pseudo-dielectric functions of our samples. It was found that the interference significantly influences on the TKE spectrum shape of sample #6. For this reason next we do not discuss the magneto-optical properties of sample #6 (being of undoubted interest). The interference contribution in the TKE spectra of the other samples is insignificant.

In order to compare the features in the discussed magneto-optical (MO) spectra with the energy spectra of (Ga,Mn)As and published MO spectra of ferromagnetic MBE-(Ga,Mn)As [5,6,10,23–26], we calculated  $\epsilon'_1(E)$  and  $\epsilon'_2(E)$  ( $\epsilon' = \epsilon'_1 - i\epsilon'_2$ ,  $-i\epsilon' = \epsilon_{xy}$ ) as well as MCD spectra for our samples #1 – #5. The calculations were carried out using the formulae (1–3) from [32], the  $\delta_{1,2}(E)$  spectra recorded at  $T = 17$  K and two incidence angles as well as the  $\langle\epsilon_1\rangle(E)$  and  $\langle\epsilon_2\rangle(E)$  ones.<sup>2</sup>

$$\delta = a\epsilon t_1 + b\epsilon t_2 \quad (1)$$

$$a = \left( \frac{2A}{A^2 + B^2} \right) \sin 2\phi, \quad b = \left( \frac{2B}{A^2 + B^2} \right) \sin 2\phi \quad (2)$$

$$A = \epsilon_2(2\epsilon_1 \cos^2 \phi - 1), \quad (3)$$

$$B = (\epsilon_2^2 - \epsilon_1^2) \cos^2 \phi + \epsilon_1 - \sin^2 \phi$$

With the  $\epsilon'_1(E)$  and  $\epsilon'_2(E)$  dependences and  $\langle n \rangle(E)$ ,  $\langle k \rangle(E)$  those, derived from the pseudo-dielectric functions, the transmission MCD spectra at  $T = 17$  K were calculated. In so doing we employed the relation (4) obtained with the use of formulae from [33].

$$\text{MCD} \sim \frac{I^+ - I^-}{I^+ + I^-} \sim \Delta\alpha(\omega) = \alpha^-(\omega) - \alpha^+(\omega)$$

$$= -\frac{2\omega}{cl} \times \frac{n\epsilon t_2 + k\epsilon t_1}{n^2 + k^2}. \quad (4)$$

In Eq. (4)  $I^+(I^-)$  and  $\alpha^+$  ( $\alpha^-$ ) are the intensities of transmitted right (left) circularly polarized light and corresponding absorption coefficients,  $\omega$  is the angular light frequency,  $c$  is the speed of light, and  $l$  is the sample thickness. Calculated MCD spectra in arbitrary units,  $\Delta\alpha(E)$ , for some samples are shown in Fig. 4. As is seen from Fig. 4, the bands that are observed in the TKE spectra displayed in Fig. 2 are well defined in the MCD those, too. The obtained MCD spectra are substantially differ from the published spectra of LT-MBE (Ga,Mn)As samples.

The negative band around 1.5 eV and positive one around 1.8 eV have been observed in the MCD spectra of paramagnetic LT-MBE  $\text{Ga}_{1-x}\text{Mn}_x\text{As}$  samples ( $x = 0.004\text{--}0.01$ ) and these band have been attributed to the  $E_0$  and  $E_0 + \Delta_0$  transitions, respectively [5,26]. Fig. 5(a,b) shows the well-known scheme of the states in the valence and conduction bands of (Ga,Mn)As split by the exchange interaction. The  $E_0$  and  $E_0 + \Delta_0$  transitions are marked by numbers 1 and 2 in Fig. 5(b). The positive band near 3.0 eV has been explained in Ref. [5,26] by the merging of two structures conditioned by the  $E_1$  and  $E_1 + \Delta_1$  transitions. The spectra of ferromagnetic (Ga,Mn)As layers with metallic conductivity investigated in Ref. [6,10,23–25] represent a broad positive band ( $E \approx 1.3\text{--}2.4$  eV) with two peculiarities.

In the framework of the “valence-band” model of ferromagnetism such a character of the MCD spectra is explained by the Fermi level shifting into the valence band, which results in changing the transitions 1 sequence compared to one shown in Fig. 5(b).

<sup>2</sup> The spectral width of the interference bands in the optical spectra in Fig. 1 is much large than the shift of the GaAs absorption edge when cooling from 300 to 17 K,  $\Delta E_g \approx 0.09$  eV [31]. Consequently, the influence of the temperature absorption edge shift on the samples optical response is insignificant. This allows us to use the  $\langle\epsilon_1\rangle(E)$  and  $\langle\epsilon_2\rangle(E)$  spectra obtained at room temperature to process the low-temperature TKE data.

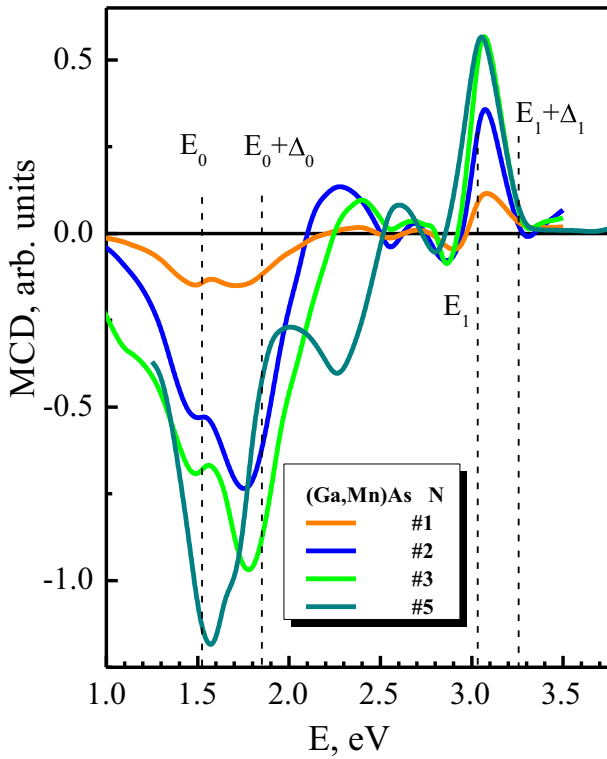


**Fig. 4.** Calculated MCD spectra,  $\Delta\alpha(E)$ , for samples #1 – #3 and #5 at  $T = 17$  K. Dashed lines indicate the energies of the transitions at the  $\Gamma$ - and L- critical points of GaAs at  $T = 22$  K [31].

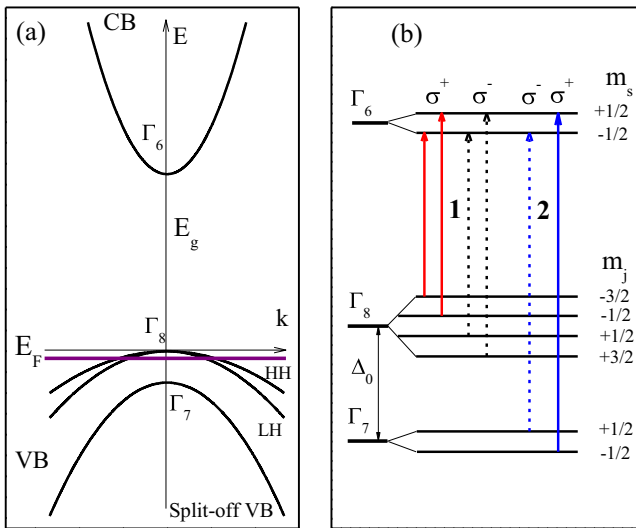


**Fig. 5.** (a) The energy band structure of (Ga,Mn)As in the vicinity of the  $\Gamma$  point. Horizontal line,  $E_F$ , indicate the location of the Fermi level below the VB top. (b) The scheme showing the exchange splitting of CB and VB at the  $\Gamma$  point, as well as the allowed optical transitions in (Ga,Mn)As in the Faraday configuration. Solid and dashed arrows represent the transitions for the right- and left-hand polarized light, ( $\sigma^+$ ,  $\Delta m_j = +1$  and  $\sigma^-$ ,  $\Delta m_j = -1$ ), respectively.

In the MCD spectra of our  $\text{Ga}_{1-x}\text{Mn}_x\text{As}$  samples #1 – #4 the broad band of negative polarity with two local extrema is observed in the region  $E \approx 1.1 - 2.25$  eV. Such the MCD spectra cannot be explained based on the scheme displayed in Fig. 5(a,b) under the assumption that the Mn and/or holes distributions through the samples are homogeneous. However it becomes possible, if it takes into account the presence of regions with different hole concentrations in consequence of inhomogeneous Mn distribution and electronic phase separation.

The negative band in the MCD spectra of samples #1 – #4 appears to be a superposition of two bands. The first MCD extremum ( $\approx 1.5$  eV) can be due to transitions 1, Fig. 5(b), from the filled or almost filled valence band to the conduction band in the regions with a low free hole concentration. In the MCD spectra of such regions, a less intense band of the positive polarity near 1.8 eV, which is conditioned by the transitions 2 from the “split-off” valence band, should also be. However, the second feature in the spectra of our samples has the opposite polarity. According to the data of Ref. [27] the Mn distribution through the samples thickness is approximately Gaussian and in addition the electronic phase separation takes place in them. Consequently, contributions from nano-sized regions with distinguishing concentrations of Mn and holes and different  $T_C$  values can be present in the magneto-optical spectra of our samples. If the hole concentration in enriched nanoregions is sufficiently high, the Fermi level lies appreciably below the valence band top (for  $p \sim 1 \times 10^{20} \text{ cm}^{-3}$  the shifting of  $\sim 250$  meV) [34]. The height of the energy barrier at the border between the hole-rich and hole-pure regions depends on the relation between the hole concentrations in these regions. Under certain conditions, the potential well formed by this barrier will represent a zero-dimensional quantum well for holes (a quantum dot) with a discrete energy spectrum. Previously, the large blue shift in the MCD spectra caused by the size quantization in heterostructure with a (Ga,Mn)As layer 2 nm thick was observed [35]. And perhaps the second feature in our MO spectra is caused by the transitions in the (Ga,Mn)As quantum dots (QDs). With an increase in the Mn concentration in the matrix, one can expect a slight blue shift of the first extremum (the Burstein-Moss shift in the “hole-pure” regions) and a red shift of the second one due to a decrease in the potential barrier at the boundary of the regions with high and low hole concentrations. If with the Mn concentration rise the QDs increase, it will also cause the red shift of the second extremum. The single negative peak of about 1.57 eV in the MCD spectrum of sample #5 may be a result of superposition of the considered bands owing to their opposite concentration shifts.

The explanation supposed for the negative MCD (and TKE) band around 1.8 eV is an assumption and further studies are needed to ascertain this band nature.

### 5. Conclusions

For the first time the optical and magneto-optical properties of Mn-doped GaAs/GaAs prepared by ion implantation with impulse laser annealing have been studied.

The enhancement of the TKE and MCD spectral features near the energies of the transitions in the critical points of the GaAs band structure has been observed that is an evidence of intrinsic ferromagnetism in the studied Mn-doped GaAs layers.

The features in the TKE and MCD spectra of the studied Mn-doped GaAs layers can be caused by inhomogeneity in the hole concentration, the Fermi level shift inward the valence band in the hole-rich nanoregions and size quantization in them.

### Acknowledgments

The work has been supported by RFBR Grant #15-02-02077 and by Helmholtz Association VHNG-713.

### References

- [1] T. Dietl, H. Ohno, *Rev. Mod. Phys.* **86** (2014) 187.
- [2] T. Jungwirth, J. Wunderlich, V. Novák, K. Olejník, B.L. Gallagher, R.P. Campion, K.W. Edmonds, A.W. Rushforth, A.J. Ferguson, P. Němec, *Rev. Mod. Phys.* **86** (2014) 855.
- [3] M. Tanaka, S. Ohya, P. Nam, Hai, *2014 Appl. Phys. Rev.* **1** (2014) 011102.

- [4] K.S. Burch, D.B. Shrekenhamer, E.J. Singley, J. Stephens, B.L. Sheu, R.K. Kawakami, P. Schiffer, N. Samarth, D.D. Awschalom, D.N. Basov, *Phys. Rev. Lett.* 97 (2006) 087208.
- [5] K. Ando, H. Saito, K.C. Agarwal, M.C. Debnath, V. Zayets, *Phys. Rev. Lett.* 100 (2008) 067204.
- [6] M. Dobrowolska, K. Tivakornasithorn, X. Liu, J.K. Furdyna, M. Berciu, K.M. Yu, W. Walukiewicz, *Nature materials* 11 (2012) 444.
- [7] I. Muneta, H. Terada, S. Ohya, M. Tanaka, *Appl. Phys. Lett.* 103 (2013) 032411.
- [8] B.C. Chapler et al., *Phys. Rev. B* 87 (2013) 205314.
- [9] T. Jungwirth, J. Sinova, T. Dietl, H. Ohno, *Phys. Rev. B* 76 (2007) 125206.
- [10] T. Jungwirth et al., *Phys. Rev. Lett.* 105 (2010) 227201.
- [11] H. Gao, C. Cernov, T. Jungwirth, J. Sinova, *Phys. Rev. B* 91 (2015) 245201.
- [12] S. Souma, L. Chen, R. Oszwaldowski, T. Sato, F. Matsukura, T. Dietl, H. Ohno, T. Takahashi, *Sci. Rep.* 6, 27266; doi: 10.1038/srep27266 (2016).
- [13] K. Ando, Springer-Verlag: Series in Solid-State Science, Magneto-Optics, Springer, Berlin, 2000, chap. 7.
- [14] H. Ohno, A. Shen, F. Matsukura, A. Oiwa, A. Endo, S. Katsumoto, H. Iye, *Appl. Phys. Lett.* 69 (1996) 363.
- [15] H. Ohno, *J. Magn. Magn. Mater.* 200 (1999) 110.
- [16] P.T. Chiu, B.W. Wessels, *Phys. Rev. B* 76 (2007) 165201.
- [17] D. Bürger, S. Zhou, M. Pandey, Ch.S. Viswanadham, J. Grenzer, O. Roshchupkina, W. Anwand, H. Reuther, V. Gottschalch, M. Helm, H. Schmidt, *Phys. Rev. B* 81 (2010) 115202.
- [18] S. Zhou, *J. Phys. D: Appl. Phys.* 48 (2015) 263001.
- [19] B.N. Zvonkov, O.V. Vikhrova, Yu.A. Danilov, E.S. Demidov, P.B. Demina, M.V. Dorokhin, Yu.N. Drozdov, V.V. Podolskii, M.V. Sapozhnikov, *J. Opt. Technol.* 75 (2008) 389.
- [20] E.A. Gan'shina, L.L. Golik, V.I. Kovalev, Z.E. Kun'kova, B.N. Zvonkov, A.N. Vinogradov, *J. Magn. Magn. Mat.* 321 (2009) 829.
- [21] E.A. Gan'shina et al., *J. Phys.: Condens. Matter* 22 (2010) 396002.
- [22] E.A. Gan'shina et al., *Solid State Phenom.* 168-169 (2011) 35.
- [23] B. Beschoten, P.A. Crowel, I. Malajovich, D.D. Awschalom, F. Matsukura, A. Shen, H. Ohno, *Phys. Rev. Lett.* 83 (1999) 3073.
- [24] J. Szczytko, W. Bardyszewski, A. Twardowski, *Phys. Rev. B* 64 (2001) 075306.
- [25] M. Berciu et al., *Phys. Rev. Lett.* 102 (2009) 247202.
- [26] H. Tanaka, W.M. Jadwisieniczak, H. Saito, V. Zayets, S. Yuasa, K. Ando, *J. Phys. D: Appl. Phys.* 47 (2014) 355001.
- [27] Ye Yuan, Chi Xu, R. Hübner, R. Jakiela, R. Böttger, M. Helm, M. Sawicki, T. Dietl, S. Zhou, *Phys. Rev. Mater.* 1 (2017) 054401.
- [28] V.I. Kovalev, A.I. Rukovichnikov, S.V. Kovalev, V.V. Kovalev, *Instrum. Exp. Tech.* 57 (2014) 607.
- [29] H. Fujiwara, *Spectroscopic Ellipsometry. Principles and Applications*, Wiley, Chichester, 2007, p. 189.
- [30] E.D. Palik, Gallium Arsenide, in: E.D. Palik (Ed.), *Handbook of Optical Constants of Solids*, Academic Press, Orlando, 1985, pp. 429–449.
- [31] P. Lautenschlager, M. Garriga, S. Logothetidis, M. Cardona, *Phys. Rev. B* 35, 9174 (1987-1).
- [32] G.S. Krinchik, *Physics of Magnetic Phenomena*, MSU Publications, Moscow, 1985, p. 299.
- [33] K. Shinagawa, in: S. Sugano, N. Kojima, *Magneto-Optics*, Springer-Verlag Series in Solid-State Science, vol. 128, chap. 5.
- [34] Y. Zhang, S. Das, Sarma, *Phys. Rev. B* 72 (2005) 125303.
- [35] H. Shimizu, M. Tanaka, *J. Appl. Phys.* 91 (2002) 7487.